

THE CIRCUMSTELLAR ENVELOPE OF ζ TAURI THROUGH OPTICAL INTERFEROMETRY

CHRISTOPHER TYCNER,¹ ARSEN R. HAJIAN,² J. T. ARMSTRONG,³ J. A. BENSON,⁴ G. C. GILBREATH,³ D. J. HUTTER,⁴
JOHN B. LESTER,⁵ D. MOZURKEWICH,³ AND T. A. PAULS³

Received 2003 August 22; accepted 2003 October 29

ABSTRACT

We present optical interferometric observations of the Be star ζ Tauri obtained using the Navy Prototype Optical Interferometer (NPOI). The multichannel capability of the NPOI allows a high-quality internal calibration of the squared visibilities corresponding to the $H\alpha$ emission from the circumstellar environment. The observations suggest a strong departure from circular symmetry and thus are described by an elliptical Gaussian model. We use a nonlinear least-squares fit to the data to obtain the likeliest parameters, and the corresponding uncertainties are determined using a Monte Carlo simulation. We obtain 3.14 ± 0.21 mas for the angular size of the major axis, -62.3 ± 4.4 for the position angle, and 0.310 ± 0.072 for the axial ratio. By comparing our results with those already in the literature, we conclude that the model parameters describing the general characteristics of the circumstellar envelope of ζ Tau appear to be stable on timescales of years. We also compare our results with the known parameters describing the binary nature of ζ Tau, and we conclude that the envelope surrounds only the primary component and is well within its Roche lobe.

Key words: stars: emission-line, Be — stars: individual (ζ Tauri) — techniques: interferometric

1. INTRODUCTION

The Be star ζ Tauri (=HR 1910) is one of the brightest stars of its type. This makes the star a very attractive target for current optical interferometers. In fact, the circumstellar envelope of ζ Tau, with a strong $H\alpha$ emission, has been observed by several such instruments, including the Mark III (Quirrenbach et al. 1994, 1997) and GI2T (Vakili et al. 1998). This paper reports observations by the Navy Prototype Optical Interferometer (NPOI).

ζ Tau is a truly interesting target because it shows very significant variations in the shape and the strength of the $H\alpha$ emission line. Although the detailed behavior of the line profile can be quite complex, the most common spectroscopic quantity used to characterize this type of variability is the ratio of the violet to red components (V/R) of the $H\alpha$ emission line. This ratio can vary on many timescales, but in the case of ζ Tau, a cyclic V/R variation on timescales of a few years is observed (Guo et al. 1995). Most recently, this type of variation has been explained with models having one-armed oscillation in a nearly Keplerian disk, such as the ones constructed by Kato (1983) and Okazaki (1991, 1997), but other models have been also proposed (see the models listed in Guo et al. 1995, and references therein). Although the first interferometric studies related to the variability of Be stars suggest that one-armed oscillations have been detected in the circumstellar disks of ζ Tau (Vakili et al. 1998) and γ Cas

(Berio et al. 1999), these first investigations do not have enough observations to model fully the spatial extent of the circumstellar material. In fact, they rely on previously determined model parameters, such as the position angle (P.A.) or the axial ratio of the line-emitting region, taken from studies based on observations from different epochs.

In this study we model the circumstellar envelope of ζ Tau as an elliptical Gaussian and compare our results with the measurements reported by Quirrenbach et al. (1997) for observations obtained from late 1991 to late 1992. We specifically concentrate on model parameters, such as the axial ratio, P.A., and angular size of the major axis, that describe the orientation and the size of the circumstellar envelope of ζ Tau. We also search for any differences that might be related to the observed changes in the shape and the overall strength of the $H\alpha$ emission from different epochs. Since ζ Tau is also a single-lined spectroscopic binary, we also look at how our size of the circumstellar envelope compares with the published binary parameters.

2. OBSERVATIONS

The observations of ζ Tau were obtained on 1999 March 1 and consist of eight individual scans. Each scan corresponds to 90 s of integration during which the fringe parameters, the squared visibilities V^2 , are measured simultaneously at three baselines and 11 spectral channels covering the region between 573 and 808 nm. The instrumental configuration of NPOI is described in detail by Armstrong et al. (1998), and the initial data reduction involved in obtaining the V^2 -values from the photon counts, for the case of a three-beam combination, is discussed by Benson et al. (1997) and Hummel et al. (1998). In addition to the observations of the target star, we have followed each scan of ζ Tau with an equivalent scan on a “check” star (for a total of eight reference scans). The check star was η Aur (=HR 1641), which is a B3 V standard star (García 1989) with no $H\alpha$ emission.

The circumstellar envelope of a typical Be star can emit radiation not only in the Balmer series, but also in other spectral lines, as well as at the continuum wavelengths due to

¹ Department of Astronomy and Astrophysics, University of Toronto, 60 St. George Street, Toronto, ON M5S 3H8, Canada; tycner@astro.utoronto.ca.

² US Naval Observatory, 3450 Massachusetts Avenue, NW, Washington, DC 20392-5420; hajian@usno.navy.mil.

³ Remote Sensing Division, Code 7210, Naval Research Laboratory, 4555 Overlook Avenue, SW, Washington, DC 20375; tom.armstrong@nrl.navy.mil, Charmaine.Gilbreath@nrl.navy.mil, dave@mozurkewich.com, pauls@nrl.navy.mil.

⁴ US Naval Observatory, Flagstaff Station, P.O. Box 1149, Flagstaff, AZ 86002; jbenon@sextans.lowell.edu, djh@nobs.navy.mil.

⁵ Department of Astronomy, University of Toronto at Mississauga, 3359 Mississauga Road North, Mississauga, ON L5L 1C6, Canada; lester@astro.utoronto.ca.

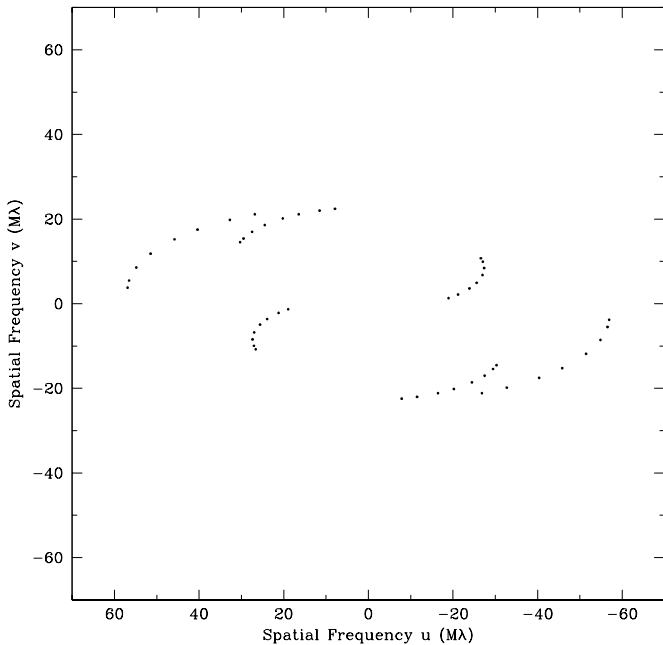


FIG. 1.—Fourier (u, v) -plane coverage at $H\alpha$ for observations of ζ Tau obtained from three simultaneous baselines in eight scans on 1999 March 1. The baselines have lengths of 18.9, 22.2, and 37.5 m, with azimuths of $-67^\circ.5$, $63^\circ.6$, and $86^\circ.0$, respectively.

the hydrogen free-free and bound-free emission (Doazan 1982). However, 2 weeks after our interferometric observations, the $H\alpha$ emission line of ζ Tau was observed to have an equivalent width (EW) of -2.064 nm, with a peak emission more than 3 times the continuum level (Banerjee, Rawat, & Janardhan 2000). Therefore, in our spectral region of interest, 573–808 nm, we concentrate on the spectral channel that contains the overwhelmingly dominant $H\alpha$ emission (see also the discussion in § 5 of Tycner et al. 2003). Figure 1 shows the Fourier (u, v) -plane coverage corresponding to the $H\alpha$ emission for all scans used in this analysis. A distinctive pattern can be seen in the plot that is caused by the changing projection of the baseline vector on the sky during the night due to Earth’s rotation.

For the observations presented in this study, the alignment of the spectral channels was such that the $H\alpha$ emission fell primarily within a single spectral channel. However, depending on the baseline used, it was either the spectral channel with a *central* wavelength at 648 or 665 nm (we will use these wavelengths as labels for the remainder of the paper). This happened because, for each baseline, the interference fringes produced at the beam combiner were dispersed onto a separate lenslet array, each with slightly different spectral alignment (see also the discussion in § 3). The nine remaining spectral channels, both at shorter (four) and longer (five) wavelengths, contain mostly continuum radiation from the star, and thus we will refer to them as the continuum channels.

3. CALIBRATION

The observed V^2 -values that we obtained after the initial reductions are not calibrated with respect to an external calibrator and therefore are degraded by many atmospheric and instrumental effects. Because the observations are obtained simultaneously over all spectral channels, we can now use the continuum channels to calibrate the V^2 -values in the channels with the $H\alpha$ contribution, which can then be used to model the circumstellar distribution of $H\alpha$ emission.

The entire calibration procedure is discussed in detail in Tycner et al. (2003), and we highlight only the major steps here. First, for a specific baseline and scan the observed squared visibilities in the nine continuum channels are expressed as

$$V_{\text{obs},i}^2 = \Gamma^2(s_i)V_p^2(s_i), \quad (1)$$

where Γ^2 is a quadratic polynomial representing the atmospheric and instrumental degradations, V_p is the visibility due to the stellar photosphere, and s_i is the spatial frequency in the radial direction from the origin of the (u, v) -plane for the i th spectral channel. We assume that the visibility due to the stellar photosphere is known or can be predicted based on the estimated angular size of the stellar component. We also assume that the contribution from the circumstellar envelope at the continuum wavelengths has a negligible effect on the observed V^2 -values.

The stellar photosphere of ζ Tau is nearly unresolved with our baselines, and therefore it is sufficient to model it with a simple uniform-disk (UD) component for which the visibilities are given by

$$V_p = V_{\text{UD}} \equiv 2 \frac{J_1(\pi\theta_{\text{UD}}s)}{\pi\theta_{\text{UD}}s}, \quad (2)$$

where J_1 is a first-order Bessel function and θ_{UD} is the angular diameter of the UD, which for ζ Tau is estimated to be 0.39 mas based on a photometric relation (see § 3.4 of Quirrenbach et al. 1997, and references therein). Therefore, when V_p^2 is known, the coefficients of the quadratic function Γ^2 can be obtained from the continuum channels using equation (1), and then the

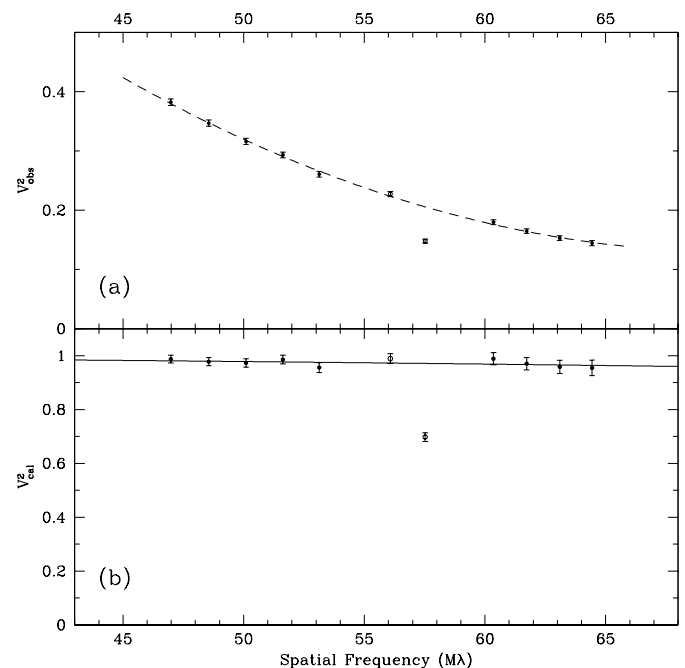


FIG. 2.—(a) Squared visibilities of ζ Tau obtained from 11 spectral channels of the 37.5 m baseline, with significant atmospheric and instrumental degradations still present. The measurements obtained from the spectral channels at 648 and 665 nm are marked with open symbols and were not used in modeling the general trend (which represents $\Gamma^2 V_{\text{UD}}^2$) with a quadratic polynomial, which is shown as a dashed line. (b) Same data as in (a) but after the correction by the Γ^2 factor. The predicted squared visibilities for the uniform stellar photospheric disk are shown as a solid line.

V^2 -values from the 648 and 665 nm channels can be calibrated according to $V_{\text{cal}}^2 = V_{\text{obs}}^2 / \Gamma^2$. In order to analyze all three baselines in the same way, neither the 648 nor the 665 nm channel was used to obtain the quadratic forms of Γ^2 for all scans, even though only one of these channels contains the contribution from the $H\alpha$ emission line at a given baseline.

Figure 2a demonstrates how effectively a quadratic polynomial (*dashed line*) describes the general trend seen in the continuum channels (*filled circles*) for one of the scans at the 37.5 m baseline. This apparent trend is mostly due to the atmospheric and instrumental degradations, but it also includes a slight contribution from the UD component. The predicted V^2 -values for the UD component are shown as a solid line in Figure 2b, and as expected, the values of V_{cal}^2 from the continuum channels resemble those of the UD model.

We can test how well a quadratic function fitted to the continuum channels describes the atmospheric and instrumental effects by completely dividing the general trend (that represents $\Gamma^2 V_{\text{UD}}^2$) out of the data. The normalized V^2 -values should cluster around unity within their uncertainties, if in fact the quadratic description is satisfactory. Figure 3 shows the residuals as a function of the central wavelengths of the

spectral channels used for all normalized observations at all three baselines. When normalized by the observational uncertainties, the majority of the residuals do fall, as expected, within a band of $\pm 1 \sigma$, indicated in the plot by the dotted lines. The only spectral channels that show significant deviations from the general trend are the ones with the contribution from the $H\alpha$ emission, the 665 nm channel for the two shortest baselines, and the 648 nm channel for the longest.

Figure 4 shows the normalized residuals for the check star η Aur (which is also nearly unresolved), and as expected, no large offsets are present in the 648 and 665 nm channels. At the same time, small systematic offsets (at the level of our slightly overestimated observational uncertainties) are visible in some spectral channels. These systematic offsets, which are spectral channel and baseline dependent, also appear to have the same general characteristics for both of our stars, and thus one might try to divide them out from our observations of the science target. However, we explain these systematic deviations as a limitation of how well we can correct for the additive bias present in each squared visibility determination. Based on our experience, the additive bias can depend on the amplitude of the squared visibility, and therefore, we decided

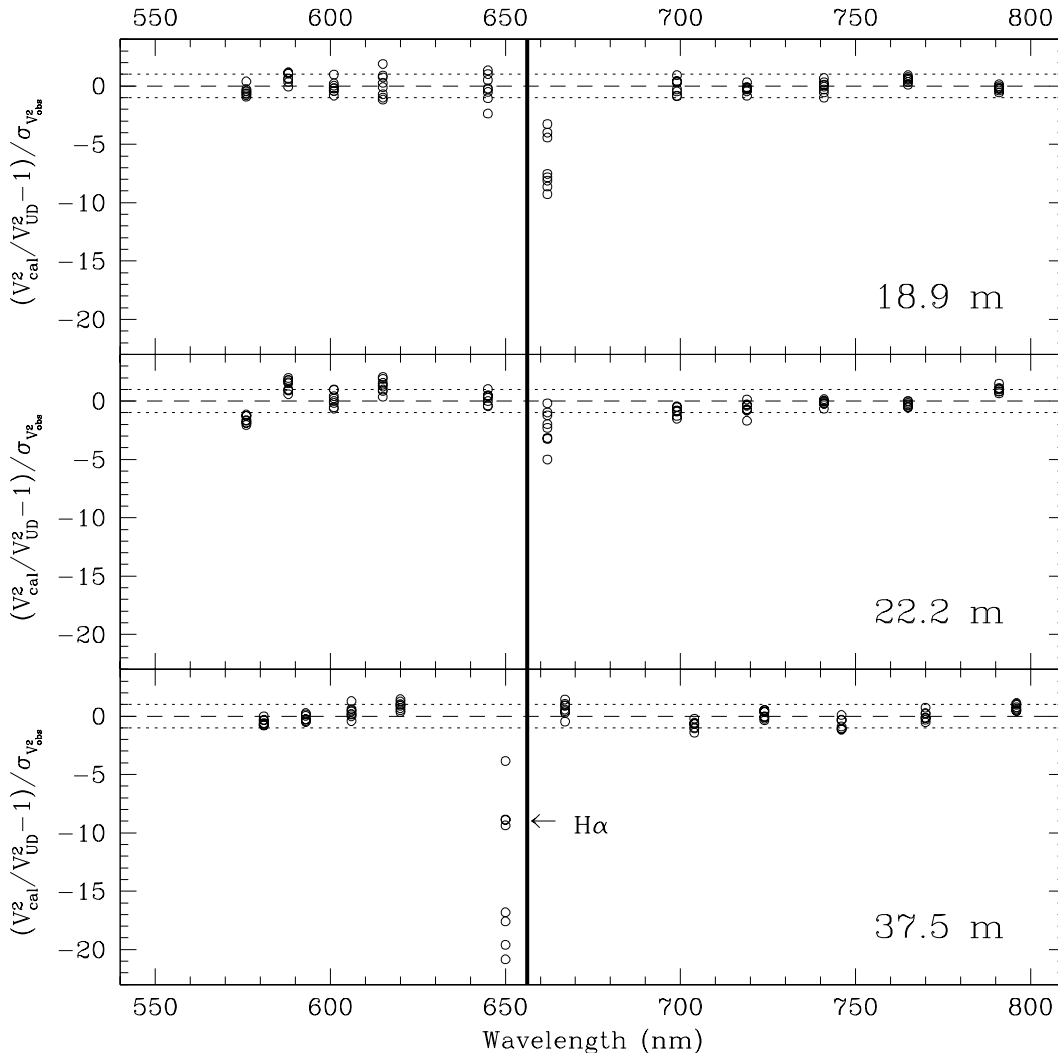


FIG. 3.—Normalized residuals of ζ Tau left after the general trend present at each scan and baseline has been divided out, plotted as a function of the *central* wavelengths of the spectral channels and with the $\pm 1 \sigma$ deviation (*dotted lines*). Each panel represents one baseline and is labeled with the physical distance between the elements that define the baseline. The position of the $H\alpha$ emission at 656.3 nm is indicated with a thick vertical line.

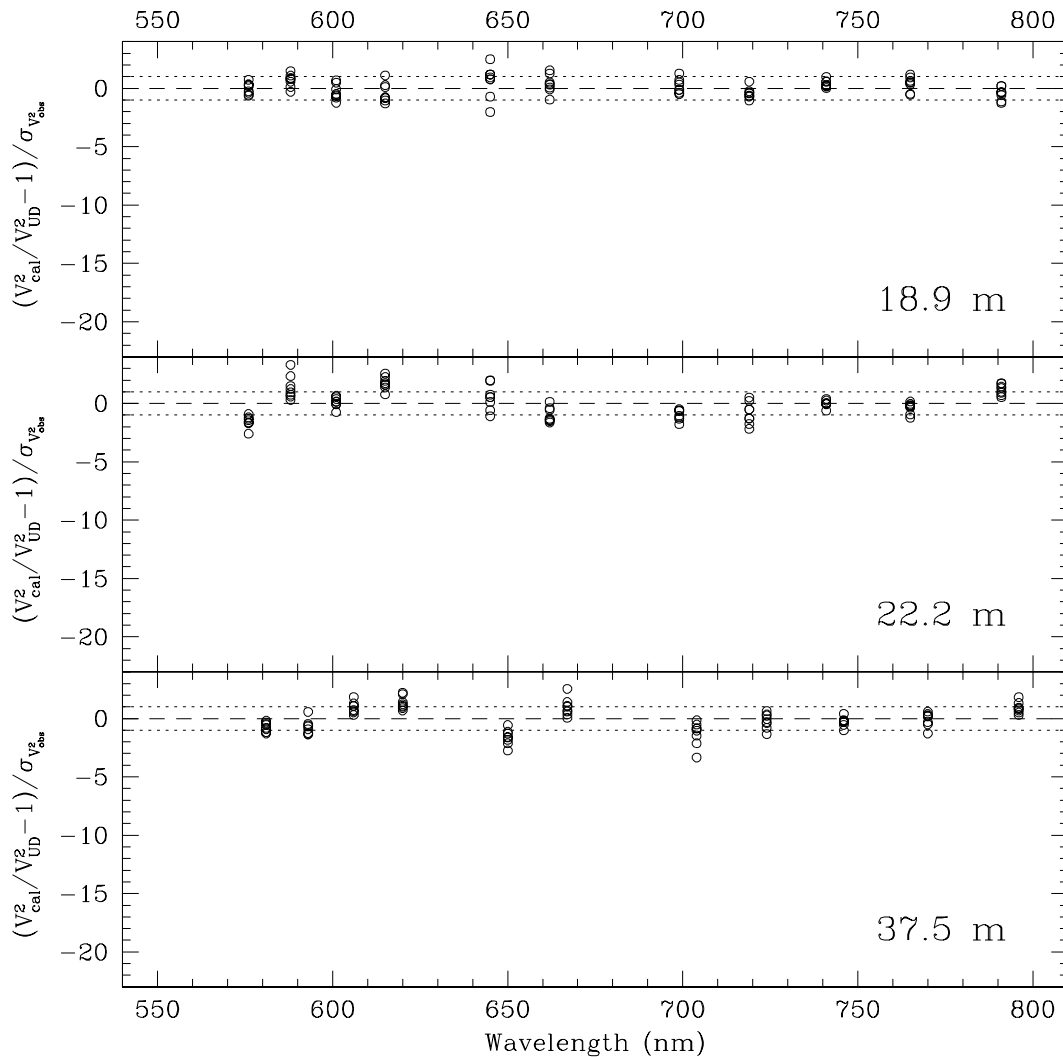


FIG. 4.—Same as Fig. 3, but for the check star η Aur

not to divide these systematic offsets out of our $H\alpha$ data (see also the discussion in § 4.3).

Because the V^2 -values due to the UD component are nearly the same for the two spectral channels at 648 and 665 nm, and because the channels have nearly the same width, we can combine the observations from both to form a single data set. More specifically, we combine the observations of ζ Tau from the 665 nm channel for the two shortest baselines with those from the 648 nm channel at the longest baseline, to produce a single data set of V^2 -values with spatial frequencies corresponding to the $H\alpha$ line (i.e., we adopt a wavelength of 656.3 nm). Figure 5 shows the calibrated squared visibilities ($V_{H\alpha}^2$) with the contribution from the $H\alpha$ emission for all three baselines and eight scans (for a total of 24 independent data points), which can now be used in model fitting.

4. MODELING THE $H\alpha$ -EMITTING ENVELOPE

4.1. Best-Fit Parameters

The spectral channels at 648 and 665 nm have widths of about 16 nm each and thus are approximately 7 times wider than the $H\alpha$ emission line (Banerjee et al. 2000). As a result, we must consider the contribution from the continuum-emitting stellar photosphere as well as the line-emitting circumstellar envelope. We treat this as a linear superposition of the two

components, and we model the calibrated V^2 -values shown in Figure 5 as

$$V_{\text{model}}^2 = [c_p V_p + (1 - c_p) V_{\text{env}}]^2, \quad (3)$$

where V_p and V_{env} are the visibilities due to the stellar photosphere and the circumstellar envelope, respectively, and c_p is a free parameter that represents the fractional contribution to the total flux of the spectral channel due to the stellar photosphere.

We model the stellar photospheric component in exactly the same way as we did for the continuum channels, with a UD that has an angular diameter of 0.39 mas (recall eq. [2]). To model the circumstellar envelope we use an elliptical Gaussian brightness distribution centered on the star. This is the simplest model that resembles the power-law density distribution falloff usually assumed for the circumstellar disks (such as the one introduced by Waters 1986) and is also the same model used by Quirrenbach et al. (1997). The normalized intensity on the sky for an elliptical Gaussian can be written as

$$I_{\text{env}}(\theta_{x'}, \theta_{y'}) = \frac{4 \ln 2}{\pi r \theta_{\text{mj}}^2} \exp \left[-\frac{(\theta_{x'}^2 / r^2 + \theta_{y'}^2)}{\theta_{\text{mj}}^2 / (4 \ln 2)} \right], \quad (4)$$

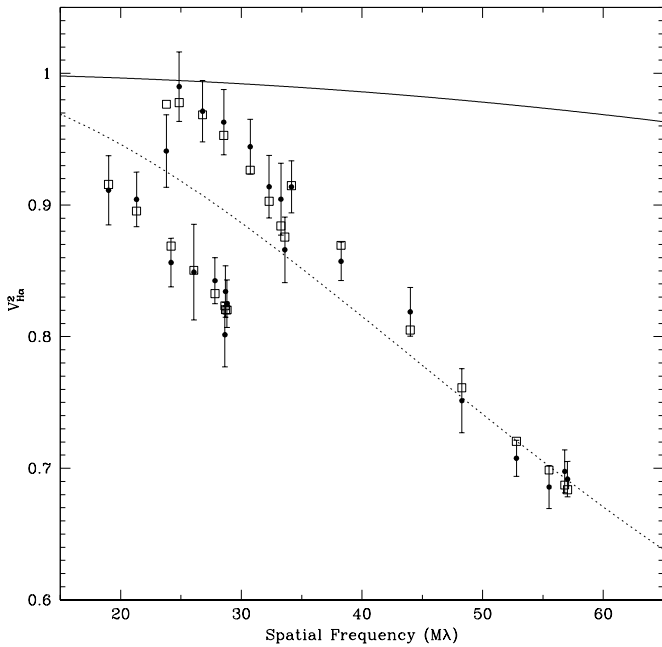


FIG. 5.—Calibrated squared visibilities of ζ Tau from the spectral channels with the $H\alpha$ emission for all three baselines and eight scans. Shown are the uniform-disk model representing the stellar photospheric disk (solid line), the best-fit circularly symmetric Gaussian model (dotted line), and the best-fit elliptical Gaussian model (squares).

where r is the axial ratio, θ_{mj} is the angular size (FWHM) of the major axis (when $r < 1$), and $(\theta_{x'}, \theta_{y'})$ are the sky coordinates in the direction of the minor and the major axes. The transformation between these coordinates and the ones in the east-west (θ_x) and north-south (θ_y) directions on the sky is

$$\theta_{x'} = \theta_x \cos \phi - \theta_y \sin \phi, \quad (5)$$

$$\theta_{y'} = \theta_x \sin \phi + \theta_y \cos \phi, \quad (6)$$

where ϕ is the P.A. (measured east from north) of the major axis.

The Fourier transform of equation (4) gives the visibility due to the Gaussian envelope and has the form

$$V_{\text{env}}(u_{x'}, v_{y'}) = \exp[-\pi^2 \theta_{\text{mj}}^2 (r^2 u_{x'}^2 + v_{y'}^2) / 4 \ln 2], \quad (7)$$

where $u_{x'}$ and $v_{y'}$ are the spatial frequencies corresponding to $\theta_{x'}$ and $\theta_{y'}$, respectively. These frequencies can be easily expressed in terms of the spatial frequencies u and v using a coordinate transformation similar to that used for the sky coordinates (i.e., $u_{x'} = u \cos \phi - v \sin \phi$ and $v_{y'} = u \sin \phi + v \cos \phi$).

Using a nonlinear least-squares fit, based on the Levenberg-Marquardt method (Press et al. 1992), we obtained the best-fit elliptical Gaussian model to the data shown in Figure 5 with a best-fit parameter set $\mathbf{P}_{\text{best}} \equiv (\theta_{\text{mj}}, r, \phi, c_p)_{\text{best}} = (3.14 \text{ mas}, 0.310, -62.3^\circ, 0.814)$ and a χ^2_{ν} (per degree of freedom) of 0.5. The uncertainties for these parameters are given in the next section along with a discussion of how they were obtained using a Monte Carlo simulation of synthetic data sets. We also note that the best-fit model parameters are influenced only slightly by the adopted angular diameter of the UD. This is because the same model (V_p) is used in the calibration of the values of $V_{H\alpha}^2$ (when the Γ^2 factor is obtained via eq. [1]) and in the modeling of the $H\alpha$ -emitting envelope (using eq. [3]).

We have tested this numerically and found that a 100% change in the assumed UD angular diameter produces changes in the best-fit parameters of less than 1%.

The elliptical Gaussian model produced a much better fit to the data than a two-parameter circularly symmetric Gaussian model, which resulted in an angular size of 1.62 mas and c_p of 0.69, but with χ^2_{ν} of 5.7. Figure 5 shows both the symmetric and the elliptical Gaussian models, along with the observed V^2 -values for the $H\alpha$ emission. It is evident from the figure that the symmetric model does not match the data. It is also apparent that the observational uncertainties are slightly overestimated, which is also suggested by $\chi^2_{\nu} < 1$.

We conclude that the elliptical Gaussian model is a significantly better match to our data than is the circular Gaussian model. The schematic representation of our best-fit elliptical Gaussian model, as it would appear on the sky, is shown in Figure 6. The polarization vector at 32° reported by McDavid (1999) is also indicated in the figure by a dashed line. Our best-fit P.A. of the major axis is at a right angle to the polarization vector, as expected for the case of electron scattering in an axisymmetric and optically thin disk (Brown & McLean 1977).

4.2. Estimating the Uncertainties

We used the Monte Carlo simulation of synthetic data sets (Press et al. 1992) to obtain the estimates for the uncertainties of the best-fit model parameters. We started with our original data set and obtained our best-fit parameters for the elliptical Gaussian model, \mathbf{P}_{best} , by minimizing χ^2 , as we have done in § 4.1. We then used these parameters to create 23,000 synthetic data sets, all with the same number of data points as our original observations, but all with different synthetic measuring errors. The synthetic errors were constructed by drawing random numbers from normal distributions, with individual widths set by the observational uncertainties of the original data points. We applied the same χ^2 minimization scheme to all synthetic data sets and obtained 23,000 synthetic best-fit values for each parameter. This gives us enough simulated parameters that the four-dimensional probability distribution is sampled sufficiently well, and we are able to measure the different projected widths of the distribution with high enough precision.

It is not possible to plot the distribution of all the solutions in the four-dimensional space, and thus Figure 7 shows the marginalized distributions in six different two-dimensional planes. The majority of the solutions fall in a localized region of the parameter space, with the highest concentration of solutions near the region defined by \mathbf{P}_{best} . The density contours shown in Figure 7 are directly proportional to the probability density functions, and therefore they provide us with information not only about the widths of the distributions, but also about the degree of correlation present between the individual pairs of parameters. We can see from the figure that most of the pairs are not correlated, with exceptions in the distributions for r versus P.A. and for c_p versus θ_{mj} , where in both cases there is a detectable correlation.

For the case in which the parameters are statistically independent (or when the correlations between parameters are ignored), the two-dimensional density contours shown in Figure 7 can be collapsed further, by allowing only one parameter to vary at a time. This is shown in Figure 8, which displays the individual probability distributions for all four model parameters. Because all four histograms resemble normal distributions, we can fit a Gaussian curve to each distribution and obtain a

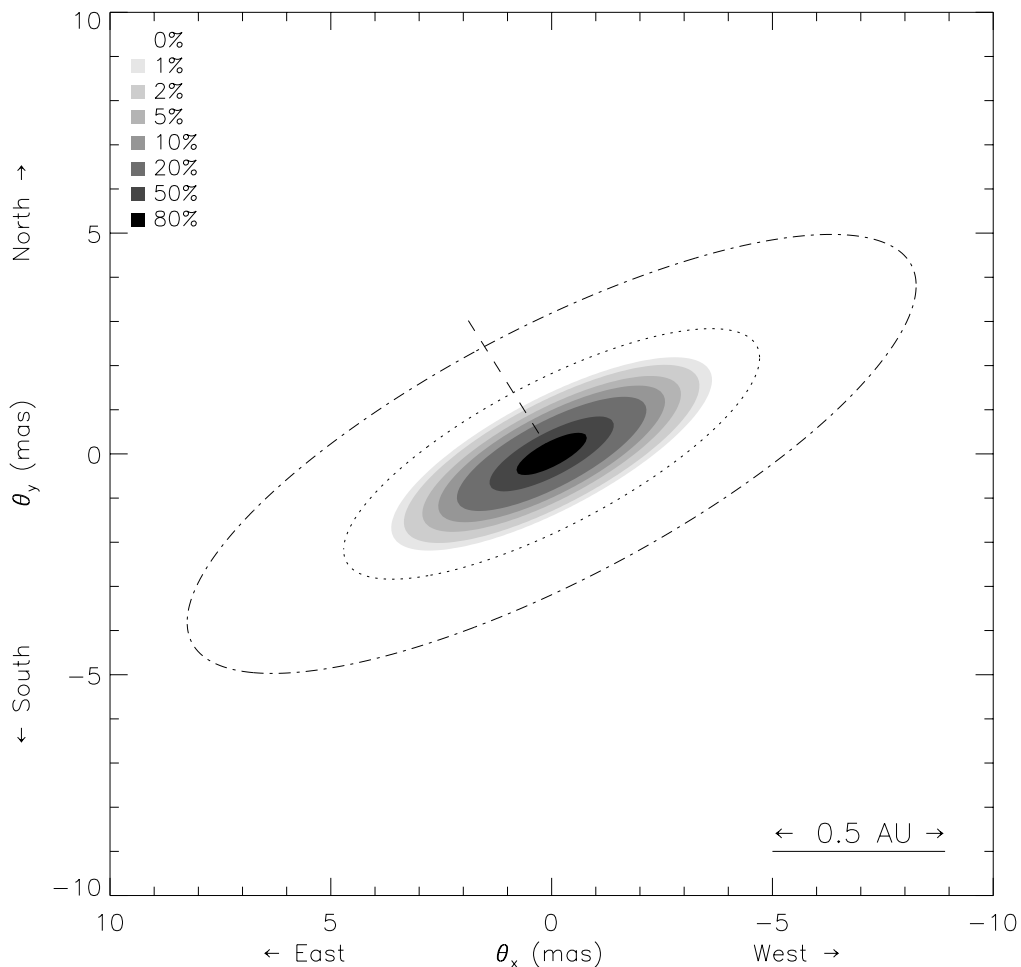


FIG. 6.—Schematic of the best-fit elliptical Gaussian model for ζ Tau. The dashed line indicates the polarization vector at 32° reported by McDavid (1999). The Roche radius of the primary star (in the plane of the disk; *dotted line*) and the projected circular orbit of the secondary component (*dash-dotted line*) are both based on the orbital parameters of Jarad (1987). The orbit neglects the small eccentricity and assumes the same orientation of the orbital plane as the circumstellar disk (see § 5.2 for more details).

corresponding standard deviation (σ) for each distribution. Based on these uncertainties, our best-fit elliptical Gaussian model has $\theta_{\text{mj}} = 3.14 \pm 0.21$ mas, $r = 0.310 \pm 0.072$, and $\phi = -62.3 \pm 4.4$. We also note that the best-fit fractional contribution c_p of 0.814 ± 0.012 compares well with our expected value of 0.84 ± 0.01 , which we estimated using the EW of the *net* H α emission (following the same procedure as Tycner et al. 2003) and by approximating the stellar photospheric contribution with the NPOI channel bandwidth (i.e., by adopting a stellar contribution of 16 ± 0.5 nm).

4.3. The Additive Bias

The data we have presented in this study might be limited not by the intrinsic scatter of the individual data points, but by the presence of an additive bias that introduces systematic offsets. The channel-to-channel variations in our calibrated data are at the $\sim 1\%$ level and appear to be baseline dependent (recall Fig. 3). This means that even if our data from the spectral channels with the H α emission are affected by the additive bias, it is unlikely that all three baselines are affected in exactly the same way. Nevertheless, to assess the significance of such a potential systematic offset on our results, we have simulated its effect on our data.

We have simulated two different cases where *all* $V^2_{\text{H}\alpha}$ values used in the original model fitting ($V^2_{\text{H}\alpha}$) were either decreased

or increased by a constant offset of 0.01. The best-fit model parameters were obtained from both data sets using the same methods applied to the original observations, and the results are listed in Table 1. Although we would intuitively expect the photospheric fraction to increase when the data are shifted to higher values, other parameters are also affected since a linear shift in V^2 -values cannot be expressed as a single adjustment of the c_p parameter (recall eq. [3]). In fact, a constant positive shift in V^2 -values corresponds to larger changes at the lower visibility values, thus making the data look “less resolved,” and produces smaller values for the angular extent of the circumstellar region, as can be seen in Table 1. The axial ratio and the P.A. of the major axis are also affected by the systematic shift, although ϕ is not very sensitive to the shift since it depends not only on the V^2 -values but also on the position angles of the individual baselines. Because r depends on the lower as well as the higher visibility values (due to the major and minor axes), and because the minor axis is not significantly resolved, it is affected slightly more by a constant shift in the data.

Based on the data in Table 1 we conclude that although our results can be affected by the presence of an additive bias, the magnitude of this effect is within our quoted uncertainties. This also justifies our use of the overestimated observational uncertainties, which yield $\chi^2_\nu < 1$ and give us final

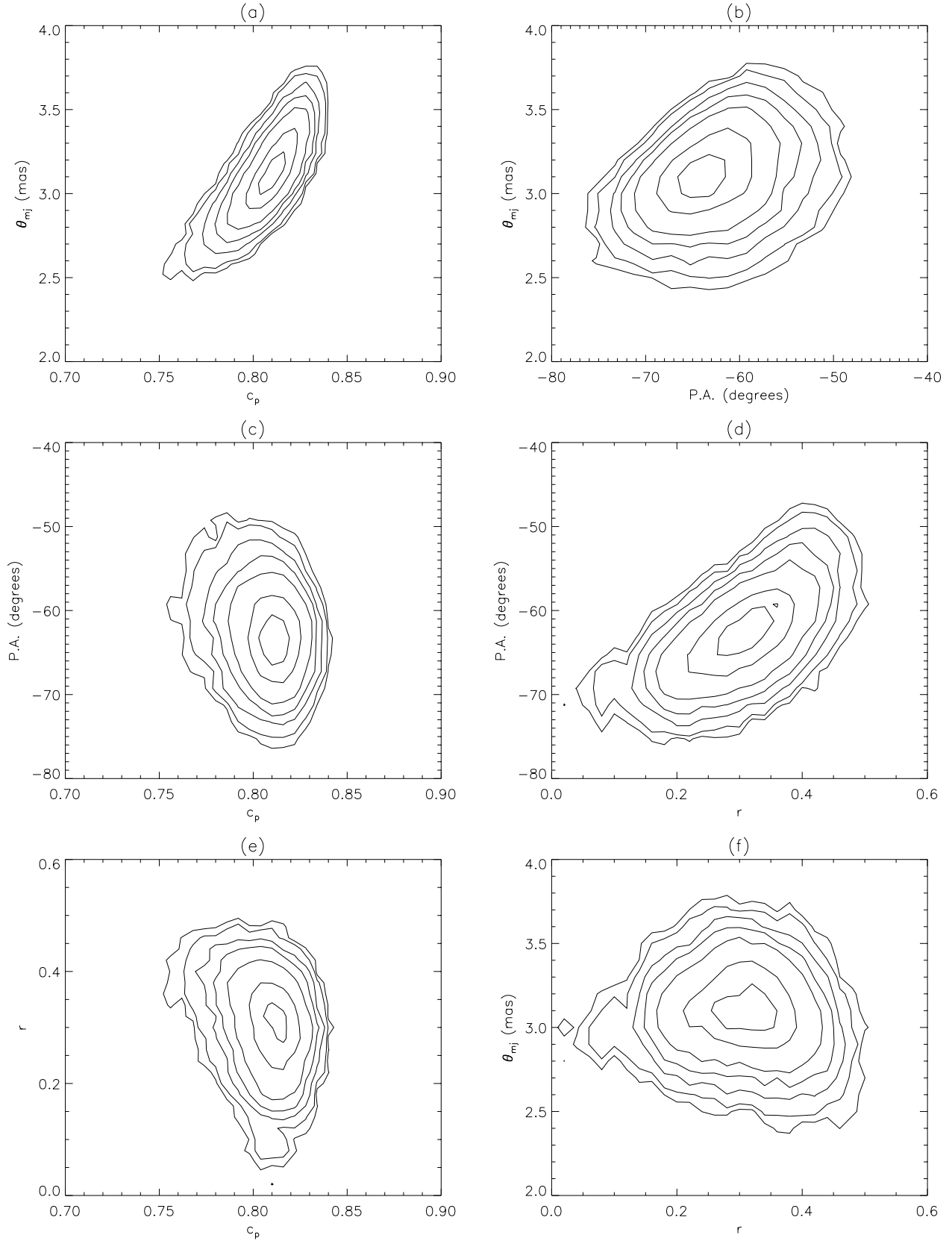


FIG. 7.—Density contour plots of the 23,000 synthetic best-fit values obtained for each of the four parameters describing the elliptical Gaussian model of ζ Tau. Each panel shows a two-dimensional view of the four-dimensional parameter space. The contour levels are at 1%, 2%, 5%, 10%, 20%, 50%, and 80% of the peak density.

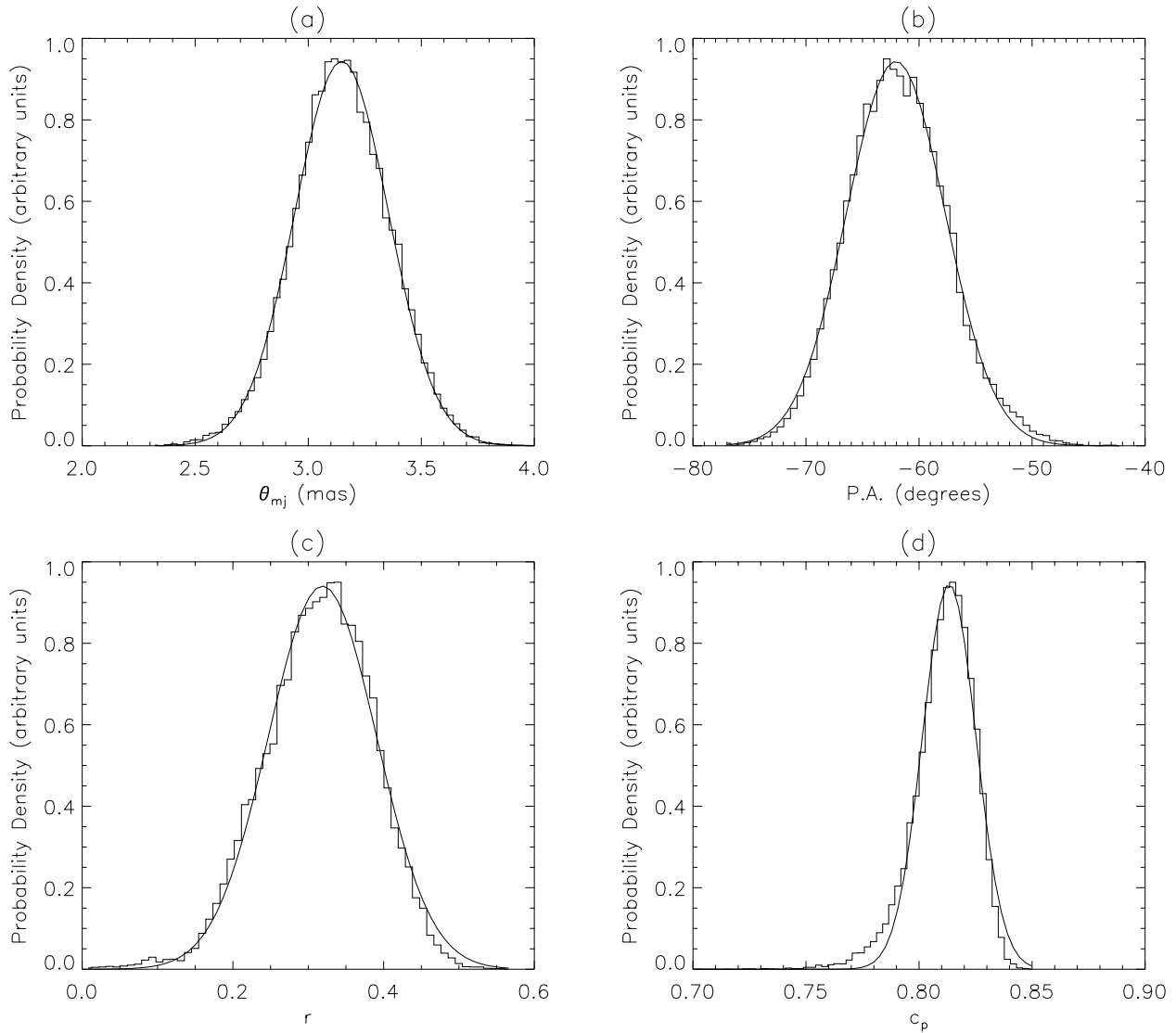


FIG. 8.—Histograms of all solutions for ζ Tau parameters plotted as a function of only one independent variable. Each panel corresponds to 23,000 best-fit values obtained from the simulated data sets. Solid lines represent the Gaussian fits to the individual distributions.

uncertainties that also account for the possible presence of such a systematic offset.

5. DISCUSSION

5.1. The Circumstellar Envelope

The circumstellar envelopes of Be stars are typically assumed to be thin, axisymmetric, circumstellar disks viewed at different angles, and therefore the axial ratio r is mostly due to a projection effect (see, e.g., Wood, Bjorkman, & Bjorkman 1997). This also means that both r and ϕ are not expected to

vary in any significant way even if variability, such as one-armed oscillation, is present in the circumstellar disk. Our best-fit values for r and ϕ of 0.310 ± 0.072 and $-62^\circ \pm 4^\circ$, which we have obtained for a single night, are in excellent agreement with the parameters reported by Quirrenbach et al. (1997) for observations obtained over a 2 month period in 1992. Their elliptical Gaussian model has an axial ratio of 0.28 ± 0.02 and P.A. of $-58^\circ \pm 4^\circ$, as well as an angular size of the major axis of 4.53 ± 0.52 mas.

It is not obvious that the apparent difference between our angular size of 3.14 ± 0.21 mas for the major axis and that of

TABLE 1
BEST-FIT MODEL PARAMETERS AT DIFFERENT LEVELS OF SIMULATED ADDITIVE BIAS

Type of Data	θ_{mj} (mas)	r	ϕ (deg)	c_p	χ^2_ν
$V_{H\alpha}^2 + 0.01$	3.01 ± 0.24	0.211 ± 0.120	-64.5 ± 4.3	0.817 ± 0.015	0.5
$V_{H\alpha}^2$	3.14 ± 0.21	0.310 ± 0.072	-62.3 ± 4.4	0.814 ± 0.012	0.5
$V_{H\alpha}^2 - 0.01$	3.26 ± 0.23	0.371 ± 0.078	-60.3 ± 5.2	0.810 ± 0.012	0.5

Quirrenbach et al. (1997) is in fact real. We have performed a number of tests to try to assess the significance of this apparent difference. We have tested the null hypothesis (that the size of the disk did not change) by treating θ_{mj} as a fixed parameter in our model-fitting procedure. We used two values for θ_{mj} based on the Quirrenbach et al. (1997) results, 4.53 and 4.01 mas (best-fit value minus 1σ), and at the expense of slightly worse fits (χ^2_ν of 1.73 and 1.03, respectively) we obtained similar results for r and ϕ as before (i.e., within their quoted uncertainties). Although in both cases the best-fit values for c_p were slightly larger, they were in agreement with our predicted value of 0.84 ± 0.01 . Based on this analysis we conclude that we cannot confidently rule out the possibility that the size of the major axis was the same at the time of our observations and that of Quirrenbach et al. (1997).

At the same time there is still a possibility (at the $\sim 1\sigma$ level quoted by Quirrenbach et al. 1997) that this difference is caused by an actual change in the extent of the circumstellar disk or is due to a different spatial position of an overdensity region such as the one reported by Vakili et al. (1998). Although on 1999 March 16 the $H\alpha$ profile observed by Banerjee et al. (2000) does not show a simple double emission structure, it does show clearly that the short-wavelength side is weaker than the long-wavelength side (i.e., $V/R < 1$). This is in the same direction as the V/R of ~ 0.7 reported by Guo et al. (1995) for the same epoch as the observations of Quirrenbach et al. (1997). Based on the analysis of Vakili et al. (1998), this suggests that the overdensity region (if present) might be located in approximately the same region of the circumstellar disk and should affect the best-fit parameters of our simple elliptical models in a very similar way. On the other hand, it is interesting to note that the EW of $H\alpha$ was larger (by about 16%) during the observations by Quirrenbach et al. (1997) than at the time of our observations (see the EW measurements by Guo et al. 1995 and Banerjee et al. 2000). Therefore, if the apparent difference between our best-fit value for θ_{mj} and that reported by Quirrenbach et al. (1997) is real, then this suggests that the physical extent of the circumstellar region might be directly correlated with the strength of the $H\alpha$ emission line. A logical extension of our study would involve simultaneous NPOI and $H\alpha$ spectroscopic observations.

5.2. The Binary Component

ζ Tau is also a single-lined spectroscopic binary with a period of about 133 days and an eccentricity of ~ 0.15 (Harmanec 1984; Jarad 1987). The inclination of the axis of the orbital plane to the line of sight is estimated to be $60^\circ < i_{\text{orb}} < 90^\circ$, based on the lack of eclipses and the presence of a hump in the radial velocity curve (see Floquet et al. 1989 and references therein). A similar lower constraint can be obtained on the angle between the rotational axis of ζ Tau and the line of sight by comparing the observed rotational velocity with the critical velocity predicted for a star of the same spectral type (Floquet et al. 1989). If we assume that the elliptical Gaussian model we obtained in § 4.1 represents an axisymmetric disk, then the lower limit for the inclination angle is $i_{\text{min}} = \arccos r \sim 70^\circ$. If we also assume that the circumstellar disk is very thin, as suggested by Wood et al. (1997), we can then use this lower limit as an approximate inclination of the circumstellar disk. This inclination angle is in the same range as the inclination angles for the star and the binary orbit estimated by Floquet et al. (1989) and suggests that all three planes have roughly the same orientation.

We do not expect to detect any signature of binarity in our data, since the secondary component is likely to be much fainter than the primary. The mass of the secondary is estimated to be $1.0\text{--}1.4 M_\odot$ (Harmanec 1984; Jarad 1987; Floquet et al. 1989). If it is a $1.4 M_\odot$ main-sequence star, it would be an F star with $M_V \sim 3$ (Gray 1992, p. 431). From the *Hipparcos* distance (ESA 1997) of 128 ± 19 pc and the apparent V magnitude of 3.0, the M_V of the primary is -2.5 ± 0.3 , or 5 mag brighter than the secondary. For this magnitude difference, the variation in V^2 as a function of spatial frequency would be at most at the $\sim 2\%$ level. Because spatial frequency is proportional to λ^{-1} on a given baseline, such variations would show up as variations in V^2 versus λ in the continuum channels. We see no variations above the 2% level in any of our scans, which is consistent with the expected magnitude difference.

Although we cannot detect the secondary component of the binary directly, we can still obtain an interesting result if we assume that the inclination angle of the orbital plane of the binary is the same as that of the circumstellar disk and use the published results from spectroscopy. Jarad (1987) estimated the basic parameters of the binary system of ζ Tau for various choices of the inclination angle (assuming that $M_{\text{primary}} \approx 11.2 M_\odot$) and for $i = 70^\circ$ predicts a binary separation of $254 \pm 20 R_\odot$ and a Roche radius (R_{Roche}) of the primary of $144 \pm 12 R_\odot$, which is obtained when the Roche lobe is approximated with a sphere of the same volume. At the distance of ζ Tau of 128 ± 19 pc, the binary separation and R_{Roche} become 9.2 ± 1.5 and 5.3 ± 0.9 mas, respectively. Figure 6 shows a schematic representation of the projected circular orbit of the secondary component (we neglect the small eccentricity) and the extent of the Roche radius in the plane of the disk, along with our best-fit elliptical Gaussian model.

The inferred binary separation is large enough to place the secondary component outside the circumstellar disk, in agreement with many models (see, e.g., Castle 1977). Furthermore, the disk lies well within the Roche radius, since the outermost disk radius, which we can take to be the 1% level of our Gaussian model, is ~ 4 mas, which suggests that the disk may be truncated by tidal interaction with the secondary. If this is the case, we would not expect to find any strong radio emission from a region much more extended than the $H\alpha$ -emitting region (in fact, Taylor et al. 1990 did not detect any radio emission for the ζ Tau system). The ζ Tau system might be one of the few Be stars for which the presence of a nearby companion limits the extent of the circumstellar disk.

6. SUMMARY

We have fitted an elliptical Gaussian model to interferometric observations of ζ Tau obtained on 1999 March 1 with the NPOI and have shown that it effectively describes our data. We have also shown that a circularly symmetric Gaussian model is not capable of modeling the data. Our best-fit values for the axial ratio and P.A. of the elliptical Gaussian confirm the values reported by Quirrenbach et al. (1997) for observations obtained about 7 years earlier. We conclude that the orientation of the disk does not appear to change on timescales much longer than the orbital period of the binary. We also conclude that the circumstellar envelope is smaller than the size derived by Jarad (1987) for the Roche lobe of the primary component of the binary.

Although our best-fit value for the major-axis angular size θ_{mj} appears to be smaller than the value reported by Quirrenbach

et al. (1997), obtained when the $H\alpha$ emission was stronger, the difference is only slightly larger than the sum of the formal errors, and therefore it is difficult to assess the significance of this change. At the same time, if this difference in θ_{mj} is real, it suggests that the size of the circumstellar envelope is correlated with the strength of the $H\alpha$ emission. Further interferometric observations of this system, preferably using the same instrumental setup, should be capable of investigating the relationship between the $H\alpha$ emission strength and the characteristics of the circumstellar envelope.

The variability of ζ Tau is known from spectroscopy (see, e.g., Hanuschik et al. 1996), as well as from optical interferometry (Vakili et al. 1998), and thus it is important to acquire sufficient data to model the source characteristics on short enough timescales. We have demonstrated in this paper that satisfactory model fits can be obtained from only 12 minutes of data using a three-beam configuration, and therefore, the

NPOI is capable of detecting intensity variations in the circumstellar environments of Be stars on short timescales. This is an important and unique observational tool, especially if combined with simultaneous high spectral resolution $H\alpha$ observations, that can probe new astrophysical phenomena.

The Navy Prototype Optical Interferometer is a joint project of the Naval Research Laboratory and the US Naval Observatory, in cooperation with Lowell Observatory, and is funded by the Office of Naval Research and the Oceanographer of the Navy. This research made use of the OYSTER software package, which was written by Christian Hummel. We thank the anonymous referee for useful comments. C. T. thanks the Natural Sciences and Engineering Research Council of Canada for postgraduate scholarships.

REFERENCES

- Armstrong, J. T., et al. 1998, *ApJ*, 496, 550
 Banerjee, D. P. K., Rawat, S. D., & Janardhan, P. 2000, *A&AS*, 147, 229
 Benson, J. A., et al. 1997, *AJ*, 114, 1221
 Berio, P., et al. 1999, *A&A*, 345, 203
 Brown, J. C., & McLean, I. S. 1977, *A&A*, 57, 141
 Castle, K. G. 1977, *PASP*, 89, 862
 Doazan, V. 1982, in *B Stars with and without Emission Lines*, ed A. B. Underhill & V. Doazan (NASA SP-456) (Washington: NASA), 370
 ESA. 1997, *The Hipparcos and Tycho Catalogues* (ESA SP-1200) (Noordwijk: ESA), 59
 Floquet, M., Hubert, A. M., Maillard, J.-P., Chauville, J., & Chatzichristou, H. 1989, *A&A*, 214, 295
 García, B. 1989, *Bull. Inf. CDS*, 36, 27
 Gray, D. F. 1992, *The Observation and Analysis of Stellar Photospheres* (Cambridge: Cambridge Univ. Press)
 Guo, Y., Huang, L., Hao, J., Cao, H., Guo, Z., & Guo, X. 1995, *A&AS*, 112, 201
 Hanuschik, R. W., Hummel, W., Sutorius, E., Dietle, O., & Thimm, G. 1996, *A&AS*, 116, 309
 Harmanec, P. 1984, *Bull. Astron. Inst. Czechoslovakia*, 35, 164
 Hummel, C. A., Mozurkewich, D., Armstrong, J. T., Hajian, A. R., Elias, N. M., II, & Hutter, D. J. 1998, *AJ*, 116, 2536
 Jarad, M. M. 1987, *Ap&SS*, 139, 83
 Kato, S. 1983, *PASJ*, 35, 249
 McDavid, D. 1999, *PASP*, 111, 494
 Okazaki, A. T. 1991, *PASJ*, 43, 75
 ———. 1997, *A&A*, 318, 548
 Press, W. H., Teukolsky, S. A., Vetterling, W. T., & Flannery, B. P. 1992, *Numerical Recipes in C* (2d ed.; Cambridge: Cambridge Univ. Press)
 Quirrenbach, A., et al. 1997, *ApJ*, 479, 477
 Quirrenbach, A., Buscher, D. F., Mozurkewich, D., Hummel, C. A., & Armstrong, J. T. 1994, *A&A*, 283, L13
 Taylor, A. R., Waters, L. B. F. M., Bjorkman, K. S., & Dougherty, S. M. 1990, *A&A*, 231, 453
 Tycner, C., et al. 2003, *AJ*, 125, 3378
 Vakili, F., et al. 1998, *A&A*, 335, 261
 Waters, L. B. F. M. 1986, *A&A*, 162, 121
 Wood, K., Bjorkman, K. S., & Bjorkman, J. E. 1997, *ApJ*, 477, 926